Anisotropy-assisted thermodynamic advantage of a local-spin quantum thermal machine

Chayan Purkait,[1,][*] Suman Chand [,][2] and Asoka Biswas[1]

[1]*Department of Physics, Indian Institute of Technology Ropar, Rupnagar, Punjab 140001, India*
[2]*Dipartimento di Fisica, Università di Genova, Via Dodecaneso 33, 16146, Genova, Italy*

We study quantum Otto thermal machines with a two-spin working system coupled by anisotropic interaction. Depending on the choice of different parameters, the quantum Otto cycle can function as different thermal machines, including a heat engine, refrigerator, accelerator, and heater. We aim to investigate how the anisotropy plays a fundamental role in the performance of the quantum Otto engine (QOE) operating in different timescales. We find that while the engine's efficiency increases with the increase in anisotropy for the quasistatic operation, quantum internal friction and incomplete thermalization degrade the performance in a finite-time cycle. Further, we study the quantum heat engine (QHE) with one of the spins (local spin) as the working system. We show that the efficiency of such an engine can surpass the standard quantum Otto limit, along with maximum power, thanks to the anisotropy. This can be attributed to quantum interference effects. We demonstrate that the enhanced performance of a local-spin QHE originates from the same interference effects, as in a measurement-based QOE for their finite-time operation.

I. INTRODUCTION

Recent advancements in experimental techniques have made it possible to measure and control systems at the level of a single atom and molecule. This has accelerated as the size of quantum devices shrinks rapidly. Consequently, it becomes imperative to understand the thermodynamics of quantum systems and the thermal machines (e.g., heat engines, refrigerators, heaters, accelerators) at the atomic level [1,2]. Several studies have been done in this direction [3], and it has been shown that nonclassical features, viz., quantum coherence [4–9], quantum correlation and entanglement [10–16], and nonthermal baths [17–21] can be exploited to enhance the performance of quantum thermal machines (QTMs).

To make a QTM useful for various practical applications of quantum technologies, one must have a nonvanishing power. Operating a quantum heat engine (QHE) quasistatically leads to null power generation and, therefore, finite-time operation of the QTMs becomes meaningful in this regard. In fact, such finite-time operation may exploit genuine non-classical properties in their performances [22,23]. It has been shown that the non-Markovian character of dynamics can speed up the control of a quantum system, thereby improving the power output of a thermal machine [24,25]. Also, quantum coherence can be harnessed to increase the power of QHEs [4,7,9,17,26] and the efficiency at maximum power [27], as well. Furthermore, the role of quantum internal friction on the work extraction and performance of the QHEs has been investigated [23,28–32].

The thermodynamics of spin systems has gained much interest due to its relevance as the basic building block

for quantum computing and quantum information processing [33,34]. There have been a plethora of works on thermodynamics of coupled spins, particularly as a working system for QTMs [22,29,35–44]. The coupling strength between the spin can serve as an additional control parameter for the cycle [45]. The coupling between spins can improve the engine's efficiency [35]. Entanglement and correlation between spins also play crucial roles [11,13,19,46]. The Hamiltonian of coupled spins can be easily built using state-of-the-art quantum technology, namely, trapped ions, quantum dots, etc. [47]. There are several proposals on how we can build Heisenberg's anisotropic spin interaction in the laboratory [48,49]. This makes a potential promise that the QHE can be tested in experiments using spins.

The anisotropy in the coupling between the spins adds further flexibility. The effect of such anisotropy on entanglement [50–54], teleportation [55–57], and the tripartite uncertainty bound [58] has been studied. Recently, the role of anisotropy in quantum batteries has been studied [59–61]. It was shown that the maximum power output of this battery can be enhanced by maintaining a low, yet nonzero anisotropy. However, there are only a few studies on the effects of anisotropy on the performance of QTMs, using, e.g., the LMG model [36], the Heisenberg XYZ model with the DM interaction [62], and measurement-assisted Heisenberg XY spin model [22]. All these works discuss the quasistatic performance of the QTMs. On the contrary, in this paper, we aim to investigate finite-time performance of the QHEs in the presence of the anisotropy.

Particularly speaking, we will study the performance of a quantum Otto engine (QOE), operating between two heat baths, with a two-spin working system coupled by Heisenberg's anisotropic XY interaction. Our investigation focuses on different durations of the cycle: (a) the quasistatic

---
[*]2018phz0001@iitrpr.ac.in

operation, (b) the nonadiabatic unitary stages, and (c) the incomplete thermalization in the hot isochoric stage. For anisotropic interaction between the spins, the Hamiltonian does not commute at two times, which introduces genuine quantum features in the finite-duration operation of the cycle [32]. We will investigate how anisotropy affects the engine's performance both for the quasistatic and finite-time operation of the engine. We show that the efficiency increases with the increase of the anisotropy for the quasistatic operation. For the finite-time operation, we show that irreversibility, measured by irreversible work, increases with the increase of the anisotropy, which in turn reduces the performance of the QOE.

Then we will consider a single-spin working system which is a part of the global two-spin system. We will call this single-spin a local system. A heat engine using one of the spins of the pair becomes relevant in a situation when the other spin is inaccessible or it is more challenging to manipulate it. We aim to investigate how the performance of a local-spin QHE differs from that of a single-spin QOE uncoupled to any other spin. We ask the following question: Can we get any thermodynamic advantage under such a local scenario, and our answer is affirmative. Several studies have been conducted on QHEs and refrigerators that function with a local system [35,37,39,41,63–67]. These studies primarily focused on studying the quasistatic operation, and also employed the Hamiltonian that commutes at different times. We want to explore how the anisotropic interaction and, therefore, the noncommuting nature of the Hamiltonian affects the performance of a local spin QHE. We show that for the quasistatic operation of the engine, local extractable work is more than for the case of a global system, and also the efficiency of a local spin QHE becomes more than that of a single spin QOE. We also show that in the finite-time operation, the efficiency can be enhanced further than the quasistatic limit, and the maximum power is associated with the enhanced efficiency.

The paper is organized as follows. We present our QHE model and implementation of the cycle in Sec. II. In Sec. III, we discuss the various limiting cases of duration of the QHE operation. Further, in Sec. IV, we explore the QHE operation using a local spin as the working system. In Sec. V discusses potential experimental implementations of our QHE model. Finally, we conclude our work in Sec. VI.

II. IMPLEMENTATION OF THE QUANTUM OTTO CYCLE

A. System model

We consider a system of two spins coupled by an anisotropic XY interaction, $J_x \neq J_y$, of Heisenberg type in a transverse time-dependent magnetic field $B(t)$. Here, $J_x = J(1 + \gamma)$ and $J_y = J(1 - \gamma)$ represent the coupling strengths along the x and y axes with the anisotropy parameter $0 \leqslant \gamma \leqslant 1$. The Hamiltonian that describes this system can be written as (in the unit of $\hbar = 1$) [22,30,68]

$$\hat{H}(t) = \hat{H}_0(t) + \hat{H}_I, \tag{1}$$

where $\hat{H}_0 = B(t)(\hat{\sigma}_1^z + \hat{\sigma}_2^z)$ represents the free part, $\hat{H}_I = J[(1 + \gamma)\hat{\sigma}_1^x\hat{\sigma}_2^x + (1 - \gamma)\hat{\sigma}_1^y\hat{\sigma}_2^y]$ represents the interaction
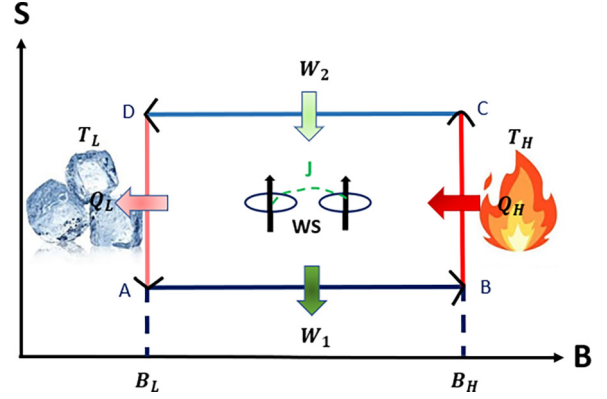
FIG. 1. Schematic diagram of the quantum Otto cycle in the entropy (S) vs magnetic field (B) plane, when it functions as a heat engine. In other types of thermal machines, the direction of heat flows and work differ.

between two spins with the coupling constant J, $J > 0$ ($J < 0$) represents the antiferromagnetic (ferromagnetic) configuration, and $\hat{\sigma}_i^{x,y,z}$ are the Pauli spin operators for the ith spin ($i \in 1, 2$). For $\gamma = 0$, the above Hamiltonian reduces to the isotropic XX model and $\gamma = 1$ gives rise to the transverse field Ising model [50]. Because $[\hat{H}_0, \hat{H}_I] \neq 0$ for $\gamma \neq 0$, it renders $[\hat{H}(t_1), \hat{H}(t_2)] \neq 0$, that introduces a true quantum feature in the operation of the finite-time QHE. This also reflects the non-Abelian nature of quantum algebra [22,32].

The eigenvalues and the corresponding eigenvectors of the total Hamiltonian [Eq. (1)] are given by

$$|\psi_{0,3}\rangle = \frac{1}{\sqrt{2}}\left(\frac{B \mp K}{\sqrt{K^2 \mp BK}}|11\rangle + \frac{\gamma J}{\sqrt{K^2 \mp BK}}|00\rangle\right),$$

$$E_{0,3} = \mp 2K,$$

$$|\psi_{1,2}\rangle = \frac{1}{\sqrt{2}}(\mp|10\rangle + |01\rangle), \quad E_{1,2} = \mp 2J, \tag{2}$$

where $K = \sqrt{B^2 + \gamma^2 J^2}$.

B. Quantum Otto cycle and thermodynamic quantities

In the following, we will discuss the implementation of the four stages of the quantum Otto cycle. The schematic diagram of the cycle is shown in Fig. 1.

1. Unitary expansion (A → B)

We assume that the cycle begins with the working system in thermal equilibrium with the cold bath at temperature $T_L = 1/\beta_L(k_B = 1)$ at point A. The corresponding thermal state of the system is $\hat{\rho}_A = e^{-\beta_L \hat{H}_1}/Z_1$, with $\hat{H}_1 = \hat{H}(0)$ and $Z_1 = \text{Tr}(e^{-\beta_L \hat{H}_1})$. During this stage, the working system stays decoupled from the cold bath, and the external magnetic field is changed from B_L to B_H ($> B_L$) following the protocol $B(t) = B_L + (B_H - B_L)(t/\tau)$, where $0 \leqslant t \leqslant \tau$ and τ is the duration of changing the magnetic field from B_L to B_H or vice versa. So at point B, the state of the system can be obtained as $\hat{\rho}_B = \hat{U}(\tau)\hat{\rho}_A\hat{U}^\dagger(\tau)$, where $\hat{U}(\tau) = \mathcal{T}e^{-i\int_0^\tau dt\hat{H}^{\exp}(t)}$ is the
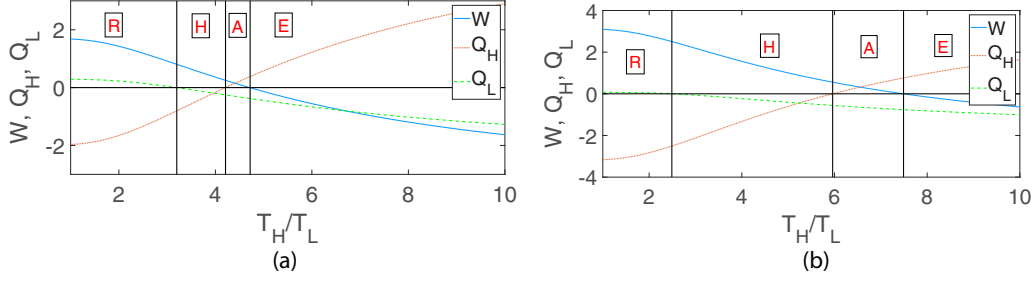
FIG. 2. Variation of the thermodynamic quantities W, Q_H, and Q_L as a function of ratio of the temperatures T_H/T_L of the hot and cold baths for different values of the anisotropy parameters (a) $\gamma = 1$ and (b) $\gamma = 0$. Symbols R, H, A, and E represent refrigerator, heater, accelerator, and engine, respectively. The other parameters are $B_L = 1$, $B_H = 4$, $J = 1$, $T_L = 1$.

time evolution operator, $\mathcal{T}$ indicates the time ordering, and $\hat{H}^{\text{exp}}(t)$ is the time-dependent Hamiltonian [Eq. (1)] with the control protocol given above. The amount of work done by the system in this stage is given by $W_1 = \langle E_B \rangle - \langle E_A \rangle$, where $\langle E_A \rangle = \text{Tr}(\hat{\rho}_A \hat{H}_1)$ and $\langle E_B \rangle = \text{Tr}(\hat{\rho}_B \hat{H}_2)$ represent the internal energies of the system at A and B, and $\hat{H}_2 = \hat{H}(\tau)$ represents the Hamiltonian of the system at B.

2. Isochoric heating (B → C)

In this stage, the working system is connected with a heat bath at temperature T_H ($> T_L$), and the external magnetic field remains fixed at a value B_H, so the Hamiltonian of the system remains fixed. Therefore, there is no work in this stage. Also, the system gets completely thermalized at a timescale t_h, which is much larger than the relaxation time t_{relax}. This means, for $t_h \gtrsim t_{\text{relax}}$, the system is incompletely thermalized in this process. After complete thermalization, the state of the working system is $\hat{\rho}_C = e^{-\beta_H \hat{H}_2}/Z_2$ at a temperature $T_H = 1/\beta_H (k_B = 1)$, with $\hat{H}_2 = \hat{H}(\tau)$ and $Z_2 = \text{Tr}(e^{-\beta_H \hat{H}_2})$. In the case of incomplete thermalization, the state of the system can be obtained by solving the master equation, as described later in Sec. III C. The system absorbs some amount of heat in this stage which can be calculated as, $Q_H = \langle E_C \rangle - \langle E_B \rangle$, where $\langle E_C \rangle = \text{Tr}(\hat{\rho}_C \hat{H}_2)$ is the internal energy of the system at C.

3. Unitary compression (C → D)

In this stage, the working system is decoupled from the hot bath and the external magnetic field is changed from B_H to B_L following the protocol $B(\tau - t)$, where $0 \leqslant t \leqslant \tau$. In this process, the state of the working system changes to $\hat{\rho}_D = \hat{V}(\tau)\hat{\rho}_C \hat{V}^\dagger(\tau)$, where $\hat{V}(\tau) = \mathcal{T}e^{-i\int_0^\tau dt \hat{H}^{\text{com}}(t)}$ is the time evolution operator with $\hat{H}^{\text{com}}(t) = \hat{H}^{\text{exp}}(\tau - t)$. The amount of work done on the system in this stage can be obtained as $W_2 = \langle E_D \rangle - \langle E_C \rangle$, where $\langle E_D \rangle = \text{Tr}(\hat{\rho}_D \hat{H}_1)$ represents the internal energy of the system at D.

4. Isochoric cooling (D → A)

In this stage, the working system is coupled to the cold bath at a temperature T_L, and the external magnetic field remains fixed at B_L. If the process is carried out for a time t_c, then the case $t_c \gg t_{\text{relax}}$ represents the timescale when the system reaches thermal equilibrium with the heat bath at the end of this process. The state of the system comes back to the initial

state ρ_A, and the system releases some amount of heat in this stage, which can be obtained as $Q_L = \langle E_A \rangle - \langle E_D \rangle$.

Operation of the quantum Otto cycle as different thermal machines

We next identify the parameter zones for which the two-spin works as a QHE. It is known that the the same system may work as different types of QTMs for different parameter zones [69,70]. We show in Fig. 2 how the work and heat vary with respect to the ratio T_H/T_L, in the presence and absence of anisotropy. From the relative signs of the work and heat, as follows, we find that the cycle can act as a heat engine, a refrigerator, an accelerator, or a heater for different regimes of T_H/T_L.

(1) Engine: $Q_H > 0$, $Q_L < 0$, $W < 0$.

(2) Refrigerator: $Q_H < 0$, $Q_L > 0$, $W > 0$.

(3) Accelerator: $Q_H > 0$, $Q_L < 0$, $W > 0$.

(4) Heater: $Q_H < 0$, $Q_L < 0$, $W > 0$.

In our paper, we will mainly focus on the heat engine operation. Total work in a complete cycle of a QHE can be obtained as $W = W_1 + W_2 = -(Q_H + Q_L)$. So, its efficiency is defined as

$$\eta = -\frac{W_1 + W_2}{Q_H} = \frac{Q_H + Q_L}{Q_H}.$$

.

III. OPERATION OF THE HEAT ENGINE IN DIFFERENT TIMEFRAMES

In this section, we will discuss the various limiting cases of duration over which the engine can be operated.

A. Quasistatic operation

We first consider that two unitary stages (expansion and compression) in the cycle are carried out over a long time such that these stages are adiabatic, i.e., there is no transition between two energy eigenstates. Two isochoric stages are also carried out for long times, so the system gets fully thermalized at the end of these stages. Such a timescale of the operation corresponds to the quasistatic cycle.

The analytical expressions of the internal energies (for derivation, see Appendix A) of the working systems at A, B,
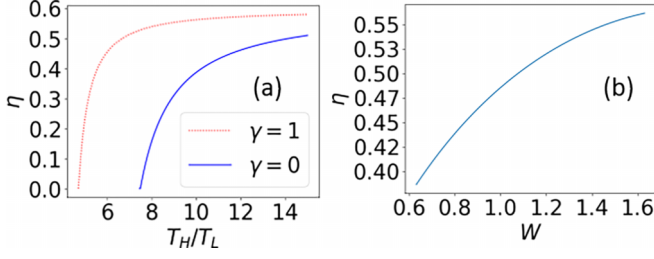
FIG. 3. (a) Variation of efficiency η as a function of the ratio of the temperatures T_H/T_L of the hot and cold baths. (b) Parametric plot of efficiency versus work as a function of anisotropy γ when $T_H = 10$. The γ varies from 0 to 1 from the left to the right. The other parameters are the same as in Fig. 2.

C, and D for a quasistatic cycle are given by

$$\langle E_{A,B} \rangle = -4K_{L,H}\frac{u_1}{Z_1} - 4J\frac{v_1}{Z_1},$$
$$\langle E_{C,D} \rangle = -4K_{H,L}\frac{u_2}{Z_2} - 4J\frac{v_2}{Z_2},\tag{3}$$

where $K_{L,H} = \sqrt{B_{L,H}^2 + \gamma^2 J^2}$ and $Z_{1,2} = 2\cosh(2K_{L,H}\beta_{L,H}) + 2\cosh(2J\beta_{L,H})$ are the partition functions. Also, $u_1 = \sinh(2K_L\beta_L)$, $u_2 = \sinh(2K_H\beta_H)$, $v_1 = \sinh(2J\beta_L)$, and $v_2 = \sinh(2J\beta_H)$.

The thermodynamic quantities of the cycle can be obtained using Eq. (3), and the work in a complete cycle is given by

$$W = W_1 + W_2 = 4(K_L - K_H)\left(\frac{u_1}{Z_1} - \frac{u_2}{Z_2}\right).\tag{4}$$

Also, heat absorption in the isochoric heating process is given by

$$Q_H = 4K_H\left(\frac{u_1}{Z_1} - \frac{u_2}{Z_2}\right) + 4J\left(\frac{v_1}{Z_1} - \frac{v_2}{Z_2}\right).\tag{5}$$

Therefore, the expression of efficiency can be obtained as

$$\eta = \frac{-W}{Q_H} = 1 - \frac{K_L(u_1 - u_2) + J(v_1 - v_2)}{K_H(u_1 - u_2) + J(v_1 - v_2)}.\tag{6}$$

From the above expression, we observe that the efficiency depends on both bath temperatures T_H and T_L, the magnetic fields B_L and B_H, and the anisotropy parameter γ. Note that for a measurement-based QOE in a coupled two-spin system [22], the hot bath is replaced by the projective measurements and the cold bath is retained. In this case, the quasistatic efficiency does not depend on the temperature of the cold bath.

In Fig. 3(a), we show the variation of the efficiency η with T_H/T_L. We find that η monotonically increases and saturates with increase in T_H/T_L. To operate the engine with higher efficiency, we choose $T_H/T_L = 10$ in the remaining part of the paper. Further, from the parametric plot of efficiency as a function of work [see Fig. 3(b)], we observe that they both increase with γ. This is contrary to the measurement-based QOE, where quasistatic efficiency decreases with the increase of γ [22]. So, we can adjust the parameters of the cycle to achieve a higher-efficiency performance of the engine.

We can also investigate the correlation between entropy and efficiency, which can provide insight into the physics behind our result. As the stages AB and CD are isentropic,
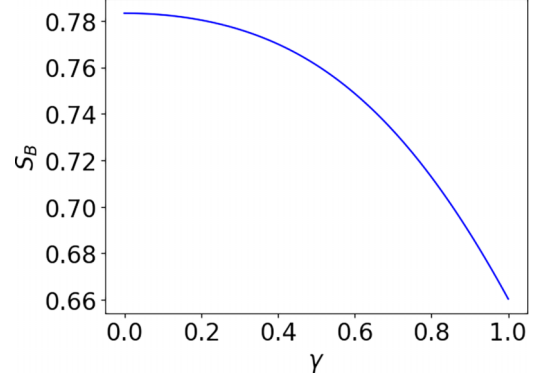
FIG. 4. Variation of entropy S_B of the global two-spin system at point B of the cycle as a function of the anisotropy parameter γ, for the quasistatic performance of the engine. We have chosen $T_H = 10$ and the other parameters are the same as in Fig. 2.

the von Neumann entropy $S = -\text{Tr}(\rho \ln \rho)$ of the working system remains unchanged during these stages, i.e., $S_B = S_A$ and $S_D = S_C$, where S_j represents the entropy of the working system at $j \in A, B, C, D$. For a working system with larger anisotropy γ, the decrease in $S_A(= S_B)$ (see Fig. 4) is much larger than the change in $S_C(= S_D)$. Therefore, the entropy difference $S_C - S_B$ (and the heat input Q_H) during the isochoric stage BC is larger for larger γ. During the stage AB, the effect of γ is more prominent because this stage occurs at a lower temperature T_L. The change in the average energy during this stage is negative, because, by increasing the magnetic field (from B_L to B_H), the eigenstates get further separated and the ground-state energy becomes more negative. This negative change in the average energy is identified as the work done by the system. During the other unitary stage CD, the work is done on the system. However, the effect of γ is not so prominent, as the higher temperature T_H obscures the small changes in eigenvalues made by changing γ. More importantly, the total work done increases more rapidly than Q_H does, with the increase in γ. Therefore, their ratio, the efficiency η, increases with γ.

B. Time-dependent unitary processes

We next consider that two unitary stages (expansion and compression) are time dependent. Nonadiabaticity appears for the shorter duration of these stages. We also assume that the isochoric stages lead to complete thermalization.

1. Thermodynamic quantities in terms of transition probability

In such a scenario, the expressions of the internal energies (for derivations, see Appendixes A and B) of the working systems at A, B, C, and D of the cycle are given by

$$\langle E_{A,C} \rangle = -4K_{L,H}\frac{u_{1,2}}{Z_{1,2}} - 4J\frac{v_{1,2}}{Z_{1,2}},$$
$$\langle E_{B,D} \rangle_\tau = -4K_{H,L}(1 - 2\xi_\tau)\frac{u_{1,2}}{Z_{1,2}} - 4J\frac{v_{1,2}}{Z_{1,2}},\tag{7}$$

where $\xi_\tau = |\langle \psi_0^{(2)} | \hat{U}(\tau) | \psi_3^{(1)} \rangle|^2 = |\langle \psi_3^{(2)} | \hat{U}(\tau) | \psi_0^{(1)} \rangle|^2 = |\langle \psi_3^{(1)} | \hat{V}(\tau) | \psi_0^{(2)} \rangle|^2 = |\langle \psi_0^{(1)} | \hat{V}(\tau) | \psi_3^{(2)} \rangle|^2$ represents the
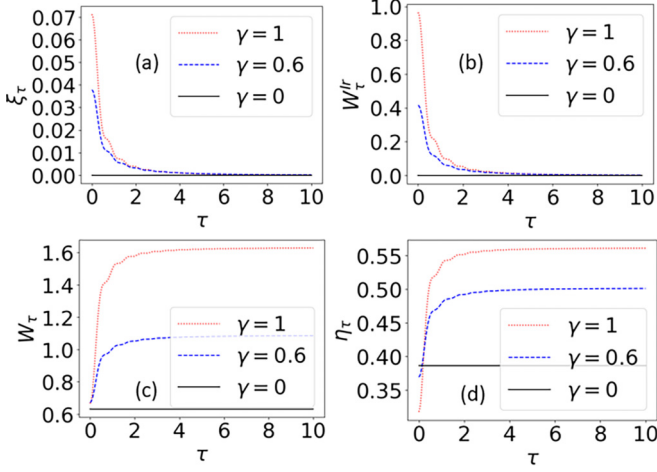
FIG. 5. Variation of (a) transition probability ξ_τ between two energy eigenstates, (b) irreversible work W_τ^{Ir}, (c) work in a complete cycle W_τ, and (d) efficiency η_τ as a function of duration τ of the unitary stages, for different values of γ. We have chosen $T_H = 10$, while the other parameters are the same as in Fig. 2.

transition probability between the associated energy levels. Here the suffix τ represents that it is a function of τ.

So, the work in a complete cycle can be obtained as

$$W_\tau = 4K_L\left[\frac{u_1}{Z_1} - (1 - 2\xi_\tau)\frac{u_2}{Z_2}\right] - 4K_H\left[(1 - 2\xi_\tau)\frac{u_1}{Z_1} - \frac{u_2}{Z_2}\right].$$
(8)

Also, heat absorbed in the isochoric heating stage is given by

$$Q_\tau = 4K_H\left[-\frac{u_2}{Z_2} - (1 - 2\xi_\tau)\frac{u_1}{Z_1}\right] + 4J\left[-\frac{v_2}{Z_2} + \frac{v_1}{Z_1}\right].$$
(9)

Therefore, the efficiency $\eta_\tau = -W_\tau/Q_\tau$ is given by

$$\eta_\tau = 1 - \frac{K_L[u_1 - (1 - 2\xi_\tau)u_2] + J[v_1 - v_2]}{K_H[(1 - 2\xi_\tau)u_1 - u_2] + J[v_1 - v_2]}.$$
(10)

The variation of the transition probability ξ_τ as a function of τ is displayed in Fig. 5(a). This dependence of ξ_τ on τ is mapped into that of η_τ via Eq. (10) and is displayed in Fig. 5(d). A similar plot for W_τ is shown in Fig. 5(c). These plots are produced using the QuTip [71] package. The work and efficiency increase with τ and eventually reaches the adiabatic (quasistatic) value, which is largest from $\gamma = 1$.

As the Hamiltonian does not commute at different times, the system cannot follow the instantaneous energy eigenstates. This induces a nonadiabatic transition between the instantaneous eigenstates of the Hamiltonian when the system is driven by an external control parameter [here $B(t)$], in finite-time unitary stages. Therefore, these stages become nonadiabatic. In this case, the extractable work in a complete cycle is reduced. In fact, an extra amount of work, which can be represented by the irreversible work, needs to be performed on the system to drive it for finite duration. Note that this irreversible work is defined as

$$W_\tau^{\mathrm{Ir}} = W_{\tau \to \infty} - W_\tau,$$
(11)

where $W_{\tau \to \infty}$ is the quasistatic work [see Eq. (5)]. This irreversible work has a finite value for finite τ. Once the driving process is completed and the system is coupled with the cold bath, the system dumps more heat into the cold bath. This degrades the overall performance of the engine in very-short-duration unitary stages, as can be seen in Figs. 5(c) and 5(d)]. This refers to the so-called quantum internal friction [28–32,72–74] and is quantified by W_τ^{Ir}. The irreversible work (W_τ^{Ir}) represents irreversibility [31] in the engine performance, which is also linked with entropy production in the system during these driven stages. We can see that the entropy (von Neumann entropy remains unchanged in a unitary process), which is defined in terms of the occupation probabilities P_n of the energy levels of a Hamiltonian $\hat{H}$ as [75] $S_{\hat{H}} = -\sum_n P_n \ln P_n$ of the system at B and C increases to a value above the quasistatic limit, if we drive the system for finite duration.

The variation of W_τ^{Ir} with respect to τ is shown in Fig. 5(b). The plot indicates that in the short-duration limit (nonadiabatic regime), the more the anisotropy (γ), the more the irreversible work. Therefore, the irreversibility increases with the increase of anisotropy (γ). For $\gamma = 1$, the system becomes an Ising spin model, which gives rise to maximum irreversibility in finite-time operation. On the other hand, for $\gamma = 0$, the system becomes a Heisenberg XX model which gives rise to a reversible operation of the cycle, irrespective of the time duration of the unitary processes.

In the adiabatic limit, i.e., $\tau \to \infty$, there is no transition between the instantaneous energy eigenstates. Therefore, we can write $\xi_\tau = |\langle\psi_0^{(2)}|\hat{U}(\tau)|\psi_3^{(1)}\rangle|^2 \overset{\tau \to \infty}{=} 0$, such that $W_\tau = W$, $W_\tau^{\mathrm{Ir}} = 0$, and $\eta_\tau = \eta$. Therefore, the expression of the quasistatic efficiency [Eq. (6)] is recovered by putting $\xi_\tau = 0$ in the expression of the finite time efficiency [Eq. (10)].

C. Time-dependent hot isochoric process

Next, we choose the hot isochoric stages to be time dependent [23,76]. Therefore, we have different thermalization scenarios of the working system depending on the time limit of this process. In the case $t_h \gg t_{\mathrm{relax}}$, the system is completely thermalized. For shorter t_h, incomplete thermalization occurs and is expected to affect the performance of the QHE.

In this case, the states of the working system at points A and B can be represented by the expressions (see Appendix A). But, to determine the state at point C, we need to solve the master equation (see below) and that, at D, the von Neumann equation becomes useful.

1. Bath model

To describe the dynamics of the system under a heat bath, the Lindblad master equation in the interaction picture can be obtained as [19,22,77]

$$\frac{\partial\hat{\rho}}{\partial t} = i[\hat{\rho}, \hat{H}(t)] + \sum_{i=1,2}\left[\Gamma(n_i + 1)\left(\hat{X}_i\hat{\rho}\hat{X}_i^+ - \frac{1}{2}\hat{X}_i^+\hat{X}_i\hat{\rho}\right.\right.$$
$$\left.\left. - \frac{1}{2}\hat{\rho}\hat{X}_i^+\hat{X}_i\right) + \Gamma n_i\left(\hat{X}_i^+\hat{\rho}\hat{X}_i - \frac{1}{2}\hat{X}_i\hat{X}_i^+\hat{\rho} - \frac{1}{2}\hat{\rho}\hat{X}_i\hat{X}_i^+\right)\right],$$
(12)
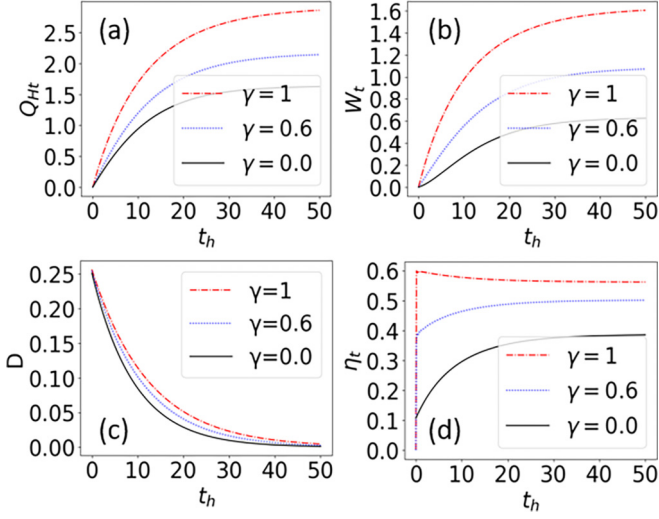
FIG. 6. Variation of (a) heat absorbed by the system Q_{Ht}, (b) work in a complete cycle W_t, (c) trace distance D, and (d) efficiency of the QHE as a function of t_h, for different values of γ. We have chosen $\Gamma = 0.1$, $T_H = 10$, while the other parameters are the same as in Fig. 2.

FIG. 7. Schematic diagram of the quantum Otto cycle on the entropy S versus magnetic field B plane when it functions as a heat engine. We consider a single local spin as a working system when the coupled two-spin global system is operated in the Otto cycle.

where we have considered that only one spin of the coupled two-spin system is interacting with a heat bath at a temperature T. The density matrix ρ represents the state of the system and the Hamiltonian $\hat{H}(t)$ is given in Eq. (1). Also, $\hat{X}_i$ represents the jump operators and their exact forms are given below. The sum over i represents the number of transitions in the system in the presence of the heat bath, and the thermal photon number distribution in the bath at the transition frequencies are $n(\omega_i) = [\exp(\frac{\hbar\omega_i}{kT}) - 1]^{-1}$. Here, Γ is the spontaneous decay rate of the system.

The jump operators of the system when only the first spin interacts with the heat bath via σ^x operator are given by [22,77]

$$X_{1,2} = \frac{1}{2}\left(\frac{B + k \mp \gamma J}{\sqrt{k^2 + Bk}}|\psi_{1,2}\rangle\langle\psi_3| + \frac{B - k \pm \gamma J}{\sqrt{k^2 - Bk}}|\psi_0\rangle\langle\psi_{2,1}|\right).$$
(13)

They signify transitions between the two energy eigenstates, involving the energy differences $\hbar\omega_1 = 2k + 2J$ and $\hbar\omega_2 = 2k - 2J$, respectively. Note that the entire two-spin system gets thermalized through the interaction of one spin with the bath. If both spins interact with the bath, we need to consider jump operators for another spin as well and the corresponding dissipator in the master equation. Then the thermalization time would be shorter than the single spin interaction, however, keeping the essential physics the same.

To understand the thermalization of the working system, we next calculate the trace distance $D(\rho, \sigma) = \frac{1}{2}\text{Tr}|\rho - \sigma|$ [76] between two states ρ, given by Eq. (A1) and σ, which is its time-evolved form obtained by solving Eq. (12). The plot of this trace distance with respect to the duration t_h of the isochoric process is shown in Fig. 6(c). We found that the thermalization slows down for larger γ [22]. Note that here $D = 0$ represents a complete thermalization.

The plots of the heat absorbed, Q_{Ht}, by the working system from the hot bath and the work done in a complete cycle as a function t_h are shown in Figs. 6(a) and 6(b). These plots show that Q_{Ht} increases with the increase of t_h and then reaches a steady value when the system is completely thermalized. Also, with the increase in Q_{Ht}, the system has more energy to perform work in a complete cycle; therefore, the work increases with t_h, and saturated for larger t_h.

The plot of the efficiency η_t with respect to t_h is shown in Fig. 6(d). For the lower value of γ, the work W_t increases slower than the significant increase of Q_{Ht}, leading to a slower increase in η_t. For $\gamma > 0.85$, in the very short value of $t_h \gtrsim 0.1$, W_t increases significantly rather than the Q_{Ht}, which gives rise to a sudden increase in efficiency and a maximum in efficiency. For larger t_h, both Q_{Ht} and W_t saturate and the efficiency η_t saturates to its quasistatic value for all values of γ (see Sec. III A).

Similar to the time-dependent hot isochoric stages, we can operate the engine under the condition that the hot isochoric stage is complete, while the cold isochoric stage is time dependent, executed in a time t_c. In this case, we would also find that the thermalization time increases with the increase of γ. All the thermodynamic quantities (heat, work, and efficiency), similar to the time-dependent hot isochoric stage, gradually increase with t_c before reaching their quasistatic values. But here, the cycle does not operate as a heat engine for smaller values of t_c, and the timescale of t_c over which the cycle does not operate as an engine increases further with γ.

IV. HEAT ENGINE OPERATION OF A LOCAL SYSTEM

In the previous section, we considered that the coupled two spin is operated in the quantum Otto cycle as illustrated in Sec. II B. In this section, we will consider a single spin, which is a part of the global system, as a working system (see Fig. 7). The primary goal is to investigate how the HE operation with a local spin differs from a QOE operating with a single-spin which is not coupled to any other spin. We want to illustrate the thermodynamic benefits of a local approach in QHE operation.

QHEs and refrigerators that function with local systems have received significant attention in recent studies [35,37,39,41,63–67]. These studies primarily focused on analyzing the quasistatic operation of the cycle and also employed the Hamiltonian that commutes at different times. In contrast, our Hamiltonian does not commute at different times [see Eq. (1)] which may give rise to some unique characteristics [22] in the finite time behavior of the QHE operating with a local spin working system. We will next explore how the noncommuting nature of the Hamiltonian impacts the performance of a local spin QHE.

The states of the local spin can be obtained by tracing out the other spin from the state of the global two-spin system at A, B, C, and D of the cycle (see Sec. II B), which will give us the states of the local spin. If the states of the global two-spin system are represented by ρ_j, where $j \in A, B, C, D$ (see Appendixes A and B), then the reduced density matrices for the first spin are given by

$$\rho_{jL} = \langle 0_2|\rho_j|0_2\rangle + \langle 1_2|\rho_j|1_2\rangle,$$

where subscript 2 represents tracing out the second spin. Therefore, the internal energies of the local spin can be obtained as $\langle E_j \rangle_L = \text{tr}(H_{jL}\rho_{jL})$, where $H_{1L} = B_L\sigma_z$ for $j \in A, D$ and $H_{2L} = B_H\sigma_z$ for $j \in B, C$ represent the Hamiltonian of the local spin.

Thermodynamic quantities of a local spin can be defined in a similar way as that of the global system (see Sec. II B). Heat absorbed in the isochoric heating process is given by $Q_{HL} = \langle E_C \rangle_L - \langle E_B \rangle_L$. The work in the unitary expansion is defined as $W_{1L} = \langle E_B \rangle_L - \langle E_A \rangle_L$, and that in the unitary compression is defined as $W_{2L} = \langle E_D \rangle_L - \langle E_C \rangle_L$, so the work in a complete cycle is $W_L = W_{1L} + W_{2L}$.

A. Quasistatic operation of the cycle

Let us consider that the cycle (see Sec. II B) for the global system is carried out quasistatically, therefore, two unitary stages are adiabatic, and the system is completely thermalized in two isochoric stages. So, the expressions (for derivation, see Appendix E) of the internal energies for the local spin are given by

$$\langle E_{A,D,B,C} \rangle_L = -2B_{L,L,H,H}(1 - a_{L,L,H,H}^2)\frac{u_{1,2,1,2}}{Z_{1,2,1,2}}, \quad (14)$$

where $a_{L,H} = \frac{B_{L,H} - K_{L,H}}{\sqrt{K_{L,H}^2 - B_{L,H}K_{L,H}}}$.

Thermodynamic quantities of the local spin are given by

$$W_L = 2\left[B_L(1 - a_L^2) - B_H(1 - a_H^2)\right]\left(\frac{u_1}{Z_1} - \frac{u_2}{Z_2}\right),$$

$$Q_{HL} = 2B_H(1 - a_H^2)\left(\frac{u_1}{Z_1} - \frac{u_2}{Z_2}\right). \quad (15)$$

1. Comparison between global and local work extraction

Now, to find the potential figure of merit of the local approach, we will compare the local work extraction with the global work extraction for the two-spin system. To do that, we will study the quantity $W_G - 2W_L$, where W_G [Eq. (5)] represents the work for the global two-spin system and W_L [Eq. (15)] represents the work for a local spin. The factor of
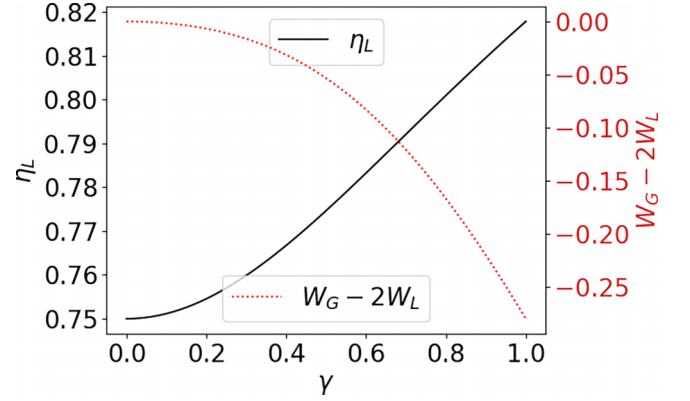
FIG. 8. On the left axis, variation of the work difference $W_G - 2W_L$ as a function of anisotropy parameter γ. On the right axis, a variation of efficiency for a local system as a function of γ. The efficiency of a single spin system QOE is 0.75 for $B_L = 1, B_H = 4$. We have chosen $T_H = 10$ and the other parameters are the same as in Fig. 2.

2 is included to consider the contribution from the two local spins. The quantity $W_G - 2W_L$ can be calculated as

$$W_G - 2W_L = 4\left[(K_H - B_H) - (K_L - B_L) + \left(B_H a_H^2 - B_L a_L^2\right)\right]$$
$$\times \left(\frac{\sinh 2K_L\beta_L}{Z_1} - \frac{\sinh 2K_H\beta_H}{Z_2}\right). \quad (16)$$

The variation of $W_G - 2W_L$ with respect to γ is shown in Fig. 8. The plot shows that $W_G < 2W_L$ if the two spins are coupled by anisotropic interaction. For the isotropic interaction, i.e., in the limit of $\gamma \to 0$, $K_H \to B_H$, $K_L \to B_L$, $a_H^2 \to 0$, and also $a_L^2 \to 0$, so $W_G = 2W_L$. The case $\gamma > 0$ gives rise to $(K_H - B_H) < (K_L - B_L)$ and also $a_H^2 < a_L^2$, so $W_G < 2W_L$, i.e., the sum of the local work from each local spin surpasses the global work from the global system. Therefore, we can say that extracting work locally is better than globally in the OOE operation with a two-spin system coupled by anisotropic interaction.

2. Comparison between the efficiencies of a local spin and a single QOE

The efficiency of the QOE cycle followed by the local spin $\eta_L = -\frac{W_L}{Q_{HL}}$ is given by

$$\eta_{Lq} = 1 - \frac{B_L(1 - a_L^2)}{B_H(1 - a_H^2)}. \quad (17)$$

The expression of the efficiency of the local spin shows that it depends on γ through $a_{L,H}$.

If a QOE operates with a single spin working system under the same physical conditions of B_L and B_H (or the same compression ratio B_L/B_H), then the expression of its efficiency is given by [70,78]

$$\eta_S = 1 - \frac{B_L}{B_H}. \quad (18)$$

We can see that $\gamma \geqslant 0$ makes the quantity $(1 - a_L^2)/(1 - a_H^2) \leqslant 1$, which gives rise to $\eta_{Lq} \geqslant \eta_S$. Therefore, as γ increases, the quantity $(1 - a_L^2)/(1 - a_H^2)$ becomes much less

than 1, which makes η_L [Eq. (17)] much larger than η_S [Eq. (18)]. For $\gamma = 0$, we get $\eta_{Lq} = \eta_S$. All of these can be seen in the plot of efficiency (Fig. 8) of the local spin QHE as a function of γ. The local spin system QHE outperforms the single spin system QOE for $\gamma > 0$. Therefore, we can say that the efficiency of a QHE operating with a local spin working system, which, in conjunction with another spin with an anisotropic interaction between a two-spin global system driven through a QOE cycle, can surpass the standard quantum Otto limit for a single spin working system.

We can also correlate the entropy of the local spin working system with the performance of the local spin QHE. When we consider a local spin (i.e., one of the two interacting spins), the entropy does not remain constant in the AB and CD stages, i.e., $S_{LB} \neq S_{LA}$ and $S_{LD} \neq S_{LC}$ for $\gamma \neq 0$, where S_{Lj} represents the entropy of a local spin at $j \in A, B, C, D$. Therefore, a local-spin heat engine, with $\gamma \neq 0$, is not exactly an Otto engine, although the two-spin system is driven through an Otto cycle. The total energy change associated with these two stages is identified as work because the global two-spin system undergoes a unitary process in these stages. Note that obtaining the reduced density matrices of the local spin at A, B, C, and D are associated with costs, which are usually not considered in the literature [35,37,39,41,63–67]. The work in the AB and CD stages becomes more for a system with larger γ. The effect of γ on the entropy changes remains somewhat similar. The entropy change, $S_{LC} - S_{LB}$, in the isochoric stage BC, increases more rapidly than $S_{LA} - S_{LD}$ when a system with larger γ is chosen. Thus, as happens in the case of a global-system heat engine, the local-spin heat engine involves more heat exchange, for larger γ. The efficiency increases with γ due to a similar reason as in the case of a global system: The work increases more than the heat input does, for larger γ.

B. Finite time operation: Time-dependent unitary processes

In this section, we consider that two unitary stages in the cycle (see Sec. II B) for the global two-spin system are carried out in a finite time τ, i.e., they are nonadiabatic in nature. However, the thermalization of the working system in the hot isochoric stage is complete. The expressions of the internal energies (for derivation, see Appendix F) of the local spin in terms of transition probabilities are given by

$$\langle E_{A,D} \rangle_L = -2B_L(1 - 2\delta_{\tau, \tau \to \infty}) \frac{u_{1,2}}{Z_{1,2}},$$

$$\langle E_{B,C} \rangle_L = -2B_H(1 - 2\lambda_{\tau, \tau \to \infty}) \frac{u_{1,2}}{Z_{1,2}}, \quad (19)$$

where $\lambda_\tau = |\langle 00|\hat{U}(\tau)|\psi_3^{(1)}\rangle|^2 = |\langle 11|\hat{U}(\tau)|\psi_0^{(1)}\rangle|^2$ and $\delta_\tau = |\langle 11|\hat{V}(\tau)|\psi_0^{(2)}\rangle|^2 = |\langle 00|\hat{V}(\tau)|\psi_3^{(2)}\rangle|^2$ represent the nonzero overlap between the basis states of a two-spin system and the instantaneous energy eigenstates. In the adiabatic limit, i.e., $\tau \to \infty$, λ_τ, and δ_τ become $\lambda_{\tau \to \infty} = a_H^2/2$ and $\delta_{\tau \to \infty} = a_L^2/2$, respectively, illustrating that finite-time average of the internal energies [see Eq. (19)] approach quasistatic average internal energies [see Eq. (14)].
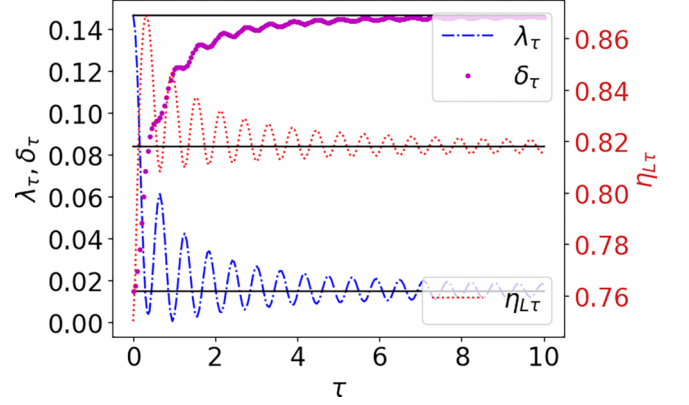
FIG. 9. Variation of the transition probability λ_τ and δ_τ on the left axis, and efficiency of a local spin on the right axis as a function of τ. The solid line on the top represents the quasistatic value of δ_τ, at the bottom represents the quasistatic value of λ_τ, and in the middle represents the quasistatic value of the local efficiency, respectively. We have chosen $\gamma = 1$ and $T_H = 10$, while the other parameters remaining are the same as in Fig. 2.

Thermodynamic quantities of the local spin are given by

$$W_{L\tau} = -2\left[\frac{u_1}{Z_1}\Big[B_H(1 - 2\lambda_\tau) - B_L(1 - 2\delta_{\tau \to \infty})\Big] \right.$$

$$\left. + \frac{u_2}{Z_2}[B_L(1 - 2\delta_\tau) - B_H(1 - 2\lambda_{\tau \to \infty})]\right],$$

$$Q_{HL\tau} = -2B_H\left[\frac{u_2}{Z_2}(1 - 2\lambda_{\tau \to \infty}) - \frac{u_1}{Z_1}(1 - 2\lambda_\tau)\right].$$

So, the efficiency, $\eta_{L\tau} = -\frac{W_{L\tau}}{Q_{HL\tau}}$, of the heat engine cycle experienced by the local spin in finite time is given by

$$\eta_{L\tau} = 1 - \frac{B_L[u_2(1 - 2\delta_\tau) - u_1(1 - 2\delta_{\tau \to \infty})]}{B_H[u_2(1 - 2\lambda_{\tau \to \infty}) - u_1(1 - 2\lambda_\tau)]}. \quad (20)$$

It can be seen that the finite-time local efficiency depends on the temperatures of the heat baths as the coefficients u_1, u_2 depend on the temperatures, whereas the quasistatic local efficiency does not depend on the temperatures of the heat baths.

Plots of the transition probabilities ($\lambda_\tau, \delta_\tau$) with respect to τ are shown in Fig. 9. If we put the value of λ_τ and δ_τ in the expression of efficiency [Eq. (20)], we get the plot of efficiency with respect to τ, which is shown in Fig. 9. This plot shows that there is an oscillatory dependence of efficiency on τ for $\gamma \neq 0$. Depending on the exact value of τ in the short time duration, a local spin system QHE can either underperform or outperform the counterpart which operates in the adiabatic limit. Thus, by adjusting the duration of the unitary stages, the efficiency of a local spin system QHE can be enhanced beyond its quasistatic limit. In a long time duration, i.e., in the adiabatic limit ($\tau \to \infty$), efficiency gradually approaches the adiabatic (quasistatic) value (see Sec. IV A). In that case, the local spin system efficiency which is represented by Eq. (20) will be reduced to Eq. (17).

In the sudden quench limit, i.e., $\tau \to 0$, the external magnetic field is changed from B_L to B_H or vice versa suddenly, in this case, both the δ_τ and λ_τ attain their
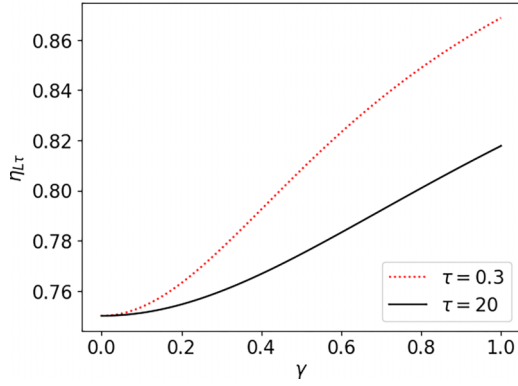
FIG. 10. Variation of efficiency of the local spin heat engine as a function of anisotropy parameter γ for different values of the unitary process time τ. $\tau = 20$ represents the adiabatic and $\tau = 0.3$ represents the nonadiabatic cases of the unitary time evolution. We have chosen $T_H = 10$ and the other parameters are the same as in Fig. 2.

sudden value, which can be obtained as $\lambda_{\tau \to 0} = |\langle 00|\psi_3^{(1)}\rangle|^2 = |\langle 11|\psi_3^{(1)}\rangle|^2$, and $\delta_{\tau \to 0} = |\langle 11|\psi_3^{(2)}\rangle|^2 = |\langle 00|\psi_3^{(2)}\rangle|^2$, as in this case $\hat{U}(\tau), \hat{V}(\tau) \to \mathbb{1}$. The engine's performance degraded in this case (see Fig. 9). Also, in the adiabatic limit, i.e., $\tau \to \infty$, both λ_τ and δ_τ reach their adiabatic value $\lambda_{\tau \to \infty}$ and $\delta_{\tau \to \infty}$. In between these two limiting cases of time, there is an oscillation in $\delta_\tau, \lambda_\tau$ with respect to τ. The oscillation in the efficiency is mainly because of the oscillation in the transition probabilities $\delta_\tau, \lambda_\tau$ in finite times of the unitary processes, which can be attributed to the interferencelike phenomena that happen between two probability amplitudes. This can be seen if we rewrite the $\lambda_\tau, \delta_\tau$ in the form given in Eq. (21),

$$
\lambda_\tau, \delta_\tau = \left| \frac{\sqrt{2}a_{H,L}}{a_{H,L}d_{H,L} - b_{H,L}c_{H,L}} \langle \psi_3^{(2)}|\hat{U}(\tau), \hat{V}(\tau)|\psi_3^{(1)}\rangle \right.
$$

$$
\left. - \frac{\sqrt{2}c_{H,L}}{a_{H,L}d_{H,L} - b_{H,L}c_{H,L}} \langle \psi_0^{(2)}|\hat{U}(\tau), \hat{V}(\tau)|\psi_3^{(1)}\rangle \right|^2,
$$

(21)

where $b_{H,L} = \frac{\gamma J}{\sqrt{k_{H,L}^2 - B_{H,L}k_{H,L}}}$, $c_{H,L} = \frac{B_{H,L} + k_{H,L}}{\sqrt{k_{H,L}^2 + B_{H,L}k_{H,L}}}$, $d_{H,L} = \frac{\gamma J}{\sqrt{k_{H,L}^2 + B_{H,L}k_{H,L}}}$. Although the oscillation in δ_τ is less prominent here compared to λ_τ for the chosen parameter domain (see Fig. 9), the oscillation in δ_τ can be found to be significant for other regions of the parameter, particularly B_H. From Fig. 9, we can see that when λ_τ goes below the $\lambda_{\tau \to \infty}$, the finite time HE outperforms its counterpart operating in the adiabatic limit ($\tau \to \infty$). Also, it can be shown that for $\gamma = 0$, the efficiency does not change with τ, because there is no interferencelike effect in this case [22].

The plot of the efficiency of the local spin QHE with respect to anisotropy parameter γ is shown in Fig. 10. It shows that the outperformance increases with the increase of γ for the finite-time operation of the engine, similar to a measurement-based QOE [22].

In fact, for the finite-time performance of the local spin QHE, the entropy at B or D at certain times, depending on the transition probabilities λ_τ and δ_τ, even goes below their quasistatic limits. As a result, finite-time work production and engine performance are better than the quasistatic limits.

1. Similarity with a measurement-based QOE

It is worth mentioning that if we are able to construct a QHE model with a transition probability between the energy eigenstates and bare basis states of the working system, then we may see an oscillation in the transition probability in finite times. This oscillation allows us to improve the performance of QHEs in finite times than the quasistatic limit. Also, this will be independent of the type of QHE model. In a recent study, it has been shown that the performance of a measurement-based QOE can be enhanced in a finite time using this type of transition probability [22]. The prescribed type of transition probability is derived from the nonselective measurement protocol. But here we obtain this from a local engine behavior perspective. Therefore, we can say that the QHE with a local working system can function like a measurement-based engine for the finite-time operation.

2. Power analysis

As we are studying the finite-time performance of the engine, it is imperative to explore the power and its relation to efficiency. The power of the local spin QHE can be defined as

$$
P_L = \frac{|W_L|}{t_h + t_c + 2\tau},
$$

(22)

where it is assumed that two isochoric stages are carried out over a long time, but not infinite time, so the states of the working system reach very close to the reference thermal states in two isochoric processes. The 3D plot of efficiency as a function of power and the duration of the unitary stages is shown in Fig. 11. From this plot, it can be seen that we can have improved efficiency (above the quasistatic limit) even at maximum power.

In most heat engine models, we sacrifice efficiency, where we need to operate the engines way below the maximum quasistatic efficiency limit, to get maximum power [79,80]. In a very short time operation, required to produce high power, different types of irreversibilities reduce work and efficiency. Again, in long-term operation, where work and efficiency both get improved but because of the long time limit, power decreases. Therefore, we need a trade-off between power and efficiency. On the contrary, in a local spin QHE, we get improved efficiency even above the quasistatic Otto limit in a very short time. This helps us to obtain maximum power with improved efficiency.

V. DISCUSSION

A similar type of analysis can be done for the refrigerator operation of the cycle. In contrast to the heat engine operation, it can be shown that the coefficient of performance (COP) of the refrigerator degrades as the anisotropy (γ) increases for the quasistatic operation of the cycle. The COP also declines
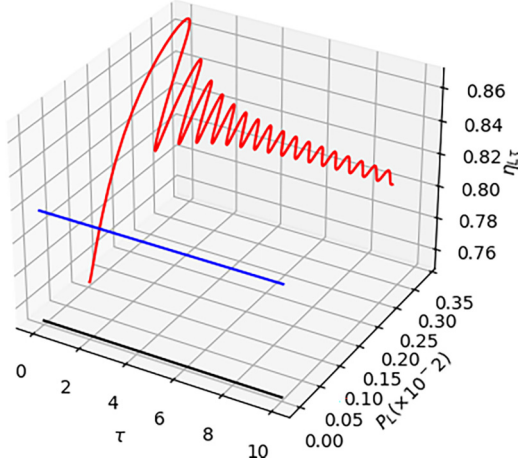
FIG. 11. Variation of efficiency of the local spin heat engine as a function of power and the time of the unitary processes τ for $\gamma = 1$. The times for the isochoric processes are $t_h = 100$, $t_c = 220$, $\Gamma = 0.1$. We have chosen $T_H = 10$, while the other parameters are the same as in Fig. 2. The blue line represents the quasistatic value of the local spin QHE's efficiency [see Eq. (17)] and the black line represents the single spin QOE's efficiency [see Eq. (18)] with zero power for the same values of the parameters as used for the finite time behavior.

when the refrigerator is operated for a finite time, which is similar to an engine.

Also, using the local analysis as that of the heat engine mentioned above, we can show that the COP of a local spin refrigerator can be enhanced in finite-time unitary processes, which is similar to the local spin QHE operation.

Heisenberg's anisotropic XY interaction between two-spin can be constructed using state-of-the-art technologies [47], particularly in NMR systems or trapped ion systems [48,49]. In a typical trapped ion system, the coupling constant J can range from a few hundred Hz to one kHz [81,82]. Also, the external magnetic field can be of the order of a few kHz [82–84]. Therefore, depending on the value of J, the time for the unitary processes τ can range from 2μs to a few ms. Also, the working system needs to be cooled at $T_L = 50$ nK and $T_H = 500$ nK.

VI. CONCLUSIONS

We have studied the quantum Otto cycle with a two-spin working system coupled by anisotropic interaction. The cycle can be operated in different thermal machine cycles, including a heat engine, refrigerator, accelerator and heater depending on different ratios of the temperatures of the hot and cold baths. Among all thermal machines, QOE is studied in different time limits. The role of anisotropy on engine performance has been investigated. We found that the engine's efficiency increases with the increase of the anisotropy parameter (γ) for the quasistatic operation of the cycle, but efficiency decreases for finite-time engine operation due to quantum internal friction. We found that the decrease in efficiency increases with the increase of γ, which signifies irreversibility in engine operation which increases with the increase of γ. In the isochoric heating process, the case of incomplete thermalization

of the working system on the thermodynamic quantities is also discussed. We observed that heat absorption and work in a complete cycle both increase with the increase in the time of the process and reach a steady value after a long time.

Further, we studied the QHE performance with a local spin working system, which is obtained by tracing out one spin from the global two-spin system. We found that the combined local work extraction from all the spins is larger than the global work extraction in the two-spin system and the difference between these two types of work extraction increases with γ. Also, for the anisotropic interaction between two-spin ($\gamma > 0$), a local spin QHE outperforms, in terms of efficiency, a single spin QOE when both functions quasistatically with the same cycle parameters. We found that the efficiency of the local spin heat engine oscillates for the finite time unitary processes of the global two-spin system. Therefore, a local spin QHE can outperform the same operating in a long time limit and this outperformance in efficiency is also associated with the maximum power output by the engine. We have shown that the oscillation in the efficiency of the local spin QHE comes due to the same origin of an interferencelike effect between two probability amplitudes as that of a nonselective measurement-based QOE.

APPENDIX A: DERIVATION OF INTERNAL ENERGIES FOR THE QUASISTATIC CASE FOR THE GLOBAL TWO-SPIN SYSTEM

At A

The Hamiltonian at point A of the cycle can be expressed as $H_A = H_1 = \sum_{i=0}^{3} E_i^{(1)} |\psi_i^{(1)}\rangle \langle \psi_i^{(1)}|$ where $\{|\psi_i^{(1)}\rangle\}$ are the eigenstates of the Hamiltonian H_1. As we consider that the system at A is in thermal equilibrium with the heat bath, the thermal density matrix is given by $\rho_A = \frac{e^{-\beta_L H_1}}{Z_1} = \sum_{i=0}^{3} P_i^L |\psi_i^{(1)}\rangle \langle \psi_i^{(1)}|$, where $P_i^L = e^{-\beta_L E_i^{(1)}}/Z_1$ is the thermal occupation probability of the ith eigenstate. So, the average internal energy at point A is given by $\langle E_A \rangle = \text{Tr}(H_1 \rho_A) = \sum_{i=0}^{3} P_i E_i^{(1)} = -4K_L \frac{u_1}{Z_1} - 4J \frac{v_1}{Z_1}$.

At B

The Hamiltonian at point B of the cycle can be expressed as $H_B = H_2 = \sum_{i=0}^{3} E_i^{(2)} |\psi_i^{(2)}\rangle \langle \psi_i^{(2)}|$, where $\{|\psi_i^{(2)}\rangle\}$ are the eigenstates of the Hamiltonian H_2. We consider that the unitary process AB is carried out adiabatically, i.e., the system follows the instantaneous eigenstates, so the state of the system at B can be written as $\rho_B = \sum_n P_n^L |\psi_n^{(2)}\rangle \langle \psi_n^{(2)}|$.

The average internal energy at point B, $\langle E_B \rangle = \text{Tr}(H_2 \rho_B)$ is given by

$$\langle E_B \rangle = P_0 E_0^{(2)} + P_3 E_0^{(2)} + P_1 E_1^{(2)} + P_2 E_2^{(2)} + P_0 E_3^{(2)} + P_3 E_3^{(2)}$$
$$= -4K_H \frac{u_1}{Z_1} - 4J \frac{v_1}{Z_1}.$$

At C

The thermal density matrix at C is given by

$$\rho_C = \frac{e^{-\beta_H H_2}}{Z_2} = \sum_{i=0}^{3} P_i |\psi_i^{(2)}\rangle\langle\psi_i^{(2)}|, \quad (A1)$$

where $P_i^H = e^{-\beta E_i^{(2)}}/Z_2$ is the thermal occupation probability of the $i^t h$ eigenstate. Similarly to point A, we can derive the expression of average energy at C which is given by $\langle E_C \rangle = \text{Tr}(H_2 \rho_c) = -4K_H \frac{u_2}{Z_2} - 4J \frac{v_2}{Z_2}$.

At D

Similarly to the unitary process AB, we consider that the unitary process CD is also carried out adiabatically. Therefore, the density matrix at the point D can be written as $\rho_D = \sum_n P_n^H |\psi_n^{(1)}\rangle\langle\psi_n^{(1)}|$.

Similarly to point B, we can derive the average internal energy at point D, which is given by

$$\langle E_D \rangle = \text{Tr}(H_1 \rho_D) = -4K_L \frac{u_2}{Z_2} - 4J \frac{v_2}{Z_2}.$$

APPENDIX B: DERIVATION OF INTERNAL ENERGIES OF THE GLOBAL TWO-SPIN SYSTEM FOR FINITE-TIME UNITARY PROCESSES

At B

The density matrix at point B after the unitary process AB can be obtained as $\rho_{B\tau} = \hat{U}(\tau)\rho_A \hat{U}^\dagger(\tau) = \sum_{i=0}^{3} P_i \hat{U}(\tau)|\psi_i^{(1)}\rangle\langle\psi_i^{(1)}|\hat{U}^\dagger(\tau)$.

The average internal energy at point B, $\langle E_B \rangle = \text{Tr}(H_2 \rho_{B\tau})$, is given by

$$\langle E_B \rangle_\tau = P_0^L E_0^{(2)}(1-\xi_\tau) + P_3^L E_0^{(2)}\xi_\tau + P_1^L E_1^{(2)}$$
$$+ P_2^L E_2^{(2)} + P_0^L E_3^{(2)}\xi_\tau + P_3^L E_3^{(2)}(1-\xi_\tau)$$
$$= -4K_H(1-2\xi_\tau)\frac{u_1}{Z_1} - 4J \frac{v_1 \beta}{Z_1}, \quad (B1)$$

where we have used the microreversibility condition $|\langle\psi_0^{(2)}|\hat{U}(\tau)|\psi_3^{(1)}\rangle|^2 = |\langle\psi_3^{(2)}|\hat{U}(\tau)|\psi_0^{(1)}\rangle|^2 = \xi_\tau$ (for proof, see Appendix D) and $|\langle\psi_0^{(2)}|\hat{U}(\tau)|\psi_0^{(1)}\rangle|^2 = |\langle\psi_3^{(2)}|\hat{U}(\tau)|\psi_3^{(1)}\rangle|^2 = 1 - \xi_\tau$. In unitary stages for a short time interval τ, nonadiabatic transitions occur between energy eigenstates that are coupled [85]. In the present case, such transitions will be induced between levels $|\psi_0\rangle$ and $|\psi_3\rangle$. So, terms like $\langle\psi_0^{(2)}|\hat{U}(\tau)|\psi_1^{(1)}\rangle$, $\langle\psi_0^{(2)}|\hat{U}(\tau)|\psi_2^{(1)}\rangle$, $\langle\psi_3^{(2)}|\hat{U}(\tau)|\psi_1^{(1)}\rangle$, etc., become zero. More details of the proof can be found in Ref. [22].

At D

The density matrix at point D after the unitary process CD is given by $\rho_{D\tau} = \hat{V}(\tau)\rho_C \hat{V}^\dagger(\tau)$. Similarly to point B, we

can derive the average internal energy at point D which is given by

$$\langle E_D \rangle_\tau = \text{Tr}(H_1 \rho_{D\tau}) = -4K_L(1-2\xi_\tau)\frac{u_2}{Z_2} - 4J \frac{v_2}{Z_2}, \quad (B2)$$

where we have used the microreversibility condition $|\langle\psi_0^{(2)}|\hat{V}(\tau)|\psi_3^{(1)}\rangle|^2 = |\langle\psi_3^{(2)}|\hat{V}(\tau)|\psi_0^{(1)}\rangle|^2 = \xi_\tau$ (for proof, see Appendix D) and $|\langle\psi_0^{(2)}|\hat{V}(\tau)|\psi_0^{(1)}\rangle|^2 = |\langle\psi_3^{(2)}|\hat{V}(\tau)|\psi_3^{(1)}\rangle|^2 = 1 - \xi_\tau$.

APPENDIX C: EQUIVALENCE OF THE TIME EVOLUTION OPERATORS IN THE UNITARY EXPANSION AND COMPRESSION PROCESSES

By utilizing the definitions (see Sec. II B) of the unitary time evolution operators in the expansion and compression stages, one can obtain the equivalence between them [76,85]:

$$\hat{U}(\tau) = \mathcal{T}\exp\left[-i\int_0^\tau H^{\exp}(t)dt\right]$$
$$= \mathcal{T}\exp\left[-i\int_0^{-\tau} H^{\exp}(-t)d(-t)\right]$$
$$= \mathcal{T}\exp\left[-i\int_\tau^0 H^{\exp}(\tau-t')d(\tau-t')\right]$$
$$= \mathcal{T}\exp\left[-i\int_0^\tau H^{\exp}(\tau-t)dt\right]$$
$$= \mathcal{T}\exp\left[-i\int_0^\tau H^{\text{com}}(t)dt\right]$$
$$= \hat{V}(\tau).$$

APPENDIX D: PROOF OF THE MICROREVERSIBILITY CONDITIONS FOR THE TOTAL TWO-SPIN SYSTEM

Using the completeness relation $\sum_{i=0}^{3} |\psi_i^{(1)}\rangle\langle\psi_i^{(1)}| = \mathbb{I}$ and the conservation of probability $|\langle\psi_0^{(2)}|\hat{U}(\tau)|\psi_3^{(1)}\rangle|^2 + |\langle\psi_3^{(2)}|\hat{U}(\tau)|\psi_3^{(1)}\rangle|^2 = 1$, we can proof the relation $|\langle\psi_3^{(2)}|\hat{U}(\tau)|\psi_0^{(1)}\rangle|^2 = |\langle\psi_0^{(2)}|\hat{U}(\tau)|\psi_3^{(1)}\rangle|^2$. For more details about the proof, see Ref. [22].

Similarly, we can prove for the unitary compression stage that $|\langle\psi_3^{(1)}|\hat{V}(\tau)|\psi_0^{(2)}\rangle|^2 = |\langle\psi_0^{(1)}|\hat{V}(\tau)|\psi_3^{(2)}\rangle|^2$. Also, using the equivalence between two unitary time evolution operators $\hat{U}(t)$ and $\hat{V}(\tau)$ (see Appendix C), we can show that $|\langle\psi_3^{(2)}|\hat{U}(\tau)|\psi_0^{(1)}\rangle|^2 = |\langle\psi_0^{(2)}|\hat{U}(\tau)|\psi_3^{(1)}\rangle|^2 = |\langle\psi_3^{(1)}|\hat{V}(\tau)|\psi_0^{(2)}\rangle|^2 = |\langle\psi_0^{(1)}|\hat{V}(\tau)|\psi_3^{(2)}\rangle|^2$.

APPENDIX E: DERIVATION OF INTERNAL ENERGIES OF A LOCAL SPIN SYSTEM FOR QUASISTATIC OPERATION

At A

The density matrix of the local spin at A, $\rho_{AL} = \langle 0_2|\rho_A|0_2\rangle + \langle 1_2|\rho_A|1_2\rangle$ is given by

$$\rho_{AL} = \frac{1}{2}\big[\big(P_0^L b_L^2 + P_1^L + P_2^L + P_3^L d_L^2\big)|0\rangle\langle 0|$$
$$+ \big(P_0^L a_L^2 + P_1^L + P_2^L + P_3^L c_L^2\big)|1\rangle\langle 1|\big], \quad (E1)$$

where P_i^L, $i \in (0, 1, 2, 3)$, are the thermal probabilities of the ith energy levels of the global system at A.

The average internal energy at point A, $\langle E_A \rangle_L = \text{Tr}(H_{L1}\rho_{AL})$, is given by

$$\langle E_A \rangle_L = \sum_{j=0,1} \langle j|(-B_L|0\rangle\langle 0| + B_L|1\rangle\langle 1|)\rho_{LA}|j\rangle$$

$$= \frac{B_L}{2}\left[P_0^L(a_L^2 - b_L^2) + P_3^L(c_L^2 - d_L^2)\right]$$

$$= B_L\left[(P_3^L - P_0^L)(1 - a_L^2)\right], \quad (E2)$$

where we have used $a_L^2 = d_L^2$, $b_L^2 = c_L^2$, and $a_L^2/2 + b_L^2/2 = 1$.

At B

The density matrix of the local spin at B, $\rho_{BL} = \langle 0_2|\rho_A|0_2\rangle + \langle 1_2|\rho_A|1_2\rangle$, is given by

$$\rho_{BL} = \frac{1}{2}\left[\left(P_0^L b_H^2 + P_1^L + P_2^L + P_3^L d_H^2\right)|0\rangle\langle 0| + \left(P_0^L a_H^2 + P_1^L + P_2^L + P_3^L c_H^2\right)|1\rangle\langle 1|\right]. \quad (E3)$$

The average internal energy at point B, $\langle E_B \rangle_L = \text{Tr}(H_{L2}\rho_{LB})$, is given by

$$\langle E_B \rangle_L = \sum_{j=0,1} \langle j|(-B_H|0\rangle\langle 0| + B_H|1\rangle\langle 1|)\rho_{LB}|j\rangle$$

$$= \frac{B_H}{2}\left[P_0^L(a_H^2 - b_H^2) + P_3^L(c_H^2 - d_H^2)\right]$$

$$= B_H\left[(P_3^L - P_0^L)(1 - a_H^2)\right], \quad (E4)$$

where we have used $a_H^2 = d_H^2$, $b_H^2 = c_H^2$, and $a_H^2/2 + b_H^2/2 = 1$.

At C

Similarly to point A, we can derive the average internal energy at point C, $\langle E_C \rangle_L = \text{Tr}(H_{L2}\rho_{CL})$, given by

$$\langle E_C \rangle_L = \frac{B_H}{2}\left[P_0^H(a_H^2 - b_H^2) + P_3^H(c_H^2 - d_H^2)\right]$$

$$= B_H\left[(P_3^H - P_0^H)(1 - a_H^2)\right], \quad (E5)$$

where P_0^H and P_3^H are the thermal probabilities zeroth and third energy levels at C.

At D

Similarly to point B, we can derive the average internal energy at D, $\langle E_D \rangle_L = \text{Tr}(H_{L1}\rho_{LD})$, given by

$$\langle E_D \rangle_L = \frac{B_L}{2}\left[P_0^H(a_L^2 - b_L^2) + P_3^H(c_L^2 - d_L^2)\right]$$

$$= B_L\left[(P_3^H - P_0^H)(1 - a_L^2)\right]. \quad (E6)$$

APPENDIX F: DERIVATION OF INTERNAL ENERGIES OF A LOCAL SPIN SYSTEM FOR FINITE TIME OPERATION

At B

The density matrix at B, $\rho_{BL\tau} = \langle 0_2|\rho_{A\tau}|0_2\rangle + \langle 1_2|\rho_{A\tau}|1_2\rangle$, is given by

$$\rho_{BL\tau} = \frac{1}{2}\left[P_1^L(|1\rangle\langle 1| + |0\rangle\langle 0|) + P_2^L(|1\rangle\langle 1| + |0\rangle\langle 0|)\right] + P_0^L\langle 0_2|\hat{U}(\tau)|\psi_0^{(1)}\rangle\langle\psi_0^{(1)}|\hat{U}^\dagger(\tau)|0_2\rangle + P_3^L\langle 0_2|\hat{U}(\tau)|\psi_3^{(1)}\rangle$$

$$\times \langle\psi_3^{(1)}|\hat{U}^\dagger(\tau)|0_2\rangle + P_0^L\langle 1_2|\hat{U}(\tau)|\psi_0^{(1)}\rangle\langle\psi_0^{(1)}|\hat{U}^\dagger(\tau)|1_2\rangle + P_3^L\langle 1_2|\hat{U}(\tau)|\psi_3^{(1)}\rangle\langle\psi_3^{(1)}|\hat{U}^\dagger(\tau)|1_2\rangle. \quad (F1)$$

The average internal energy, $\langle E_{LBt} \rangle = \text{Tr}(H_{L2}\rho_{LBt})$ is given by

$$\langle E_B \rangle_{L\tau} = \sum_{j=0,1} \langle j|(-B_H|0\rangle\langle 0| + B_H|1\rangle\langle 1|)\rho_{LB}|j\rangle$$

$$= -P_0^H B_H\left|\langle 00|\hat{U}(\tau)|\psi_0^{(1)}\rangle\right|^2 - P_3^H B_H\left|\langle 00|\hat{U}(\tau)|\psi_3^{(1)}\rangle\right|^2 + P_0^H B_H\left|\langle 11|\hat{U}(\tau)|\psi_0^{(1)}\rangle\right|^2 + P_3^H B_H\left|\langle 11|\hat{U}(\tau)|\psi_3^{(1)}\rangle\right|^2$$

$$= B_H(P_3^L - P_0^L)(1 - 2\delta_\tau), \quad (F2)$$

where we have used the microreversibility conditions (for derivation, see Appendix G) $|\langle 00|\hat{U}(\tau)|\psi_0^{(1)}\rangle|^2 = 1 - \lambda_\tau$, $|\langle 00|\hat{U}(\tau)|\psi_3^{(1)}\rangle|^2 = \lambda_\tau$, $|\langle 11|\hat{U}(\tau)|\psi_0^{(1)}\rangle|^2 = \lambda_\tau$, $|\langle 11|\hat{U}(\tau)|\psi_3^{(1)}\rangle|^2 = 1 - \lambda_\tau$.

At D

Similarly to point B, we can derive the expression of the average internal energy at D, $\langle E_D \rangle_{L\tau} = \text{Tr}(H_{L1}\rho_{DL\tau})$, given by

$$\langle E_D \rangle_{L\tau} = B_L(P_3^H - P_0^H)(1 - 2\delta_\tau), \quad (F3)$$

where we need to use the microreversibility conditions (for derivation, see Appendix G) $|\langle 00|\hat{V}(\tau)|\psi_0^{(2)}\rangle|^2 =$

$1 - \delta_\tau$, $|\langle 00|\hat{V}(\tau)|\psi_3^{(2)}\rangle|^2 = \delta_\tau$, $|\langle 11|\hat{V}(\tau)|\psi_0^{(2)}\rangle|^2 = \delta_\tau$, and $|\langle 11|\hat{V}(\tau)|\psi_3^{(2)}\rangle|^2 = 1 - \delta_\tau$.

APPENDIX G: PROOF OF THE MICRO-REVERSIBILITY CONDITION FOR THE LOCAL SPIN SYSTEM

We can proof the relation $|\langle 00|\hat{U}(\tau)|\psi_3^{(1)}\rangle|^2 = |\langle 11|\hat{U}(\tau)|\psi_0^{(1)}\rangle|^2$ using the completeness relation $\sum_{i=0}^3 |\psi_i^{(1)}\rangle\langle\psi_i^{(1)}| = \mathbb{I}$ and the conservation of probability $|\langle 00|\hat{U}(\tau)|\psi_0^{(1)}\rangle|^2 + |\langle 11|\hat{U}(\tau)|\psi_0^{(1)}\rangle|^2 = 1$, whereas other two terms $|\langle 01|\hat{U}(\tau)|\psi_0^{(1)}\rangle|^2 = 0$, and $|\langle 10|\hat{U}(\tau)|\psi_0^{(1)}\rangle|^2 = 0$.

Similarly, we can prove that $|\langle 00|\hat{V}(\tau)|\psi_3^{(2)}\rangle|^2 = |\langle 11|\hat{V}(\tau)|\psi_0^{(2)}\rangle|^2$, where we need to use the conservation of probability $|\langle 00|\hat{V}(\tau)|\psi_0^{(2)}\rangle|^2 + |\langle 11|\hat{V}(\tau)|\psi_0^{(2)}\rangle|^2 = 1$.

[1] S. Vinjanampathy and J. Anders, Contemp. Phys. **57**, 545 (2016).

[2] F. Binder, L. A. Correa, C. Gogolin, J. Anders, and G. Adesso, Fundam. Theor. Phys. **195**, 1 (2018).

[3] S. Bhattacharjee and A. Dutta, Eur. Phys. J. B **94**, 239 (2021).

[4] M. O. Scully, K. R. Chapin, K. E. Dorfman, M. B. Kim, and A. Svidzinsky, Proc. Natl. Acad. Sci. USA **108**, 15097 (2011).

[5] K. Brandner, M. Bauer, M. T. Schmid, and U. Seifert, New J. Phys. **17**, 065006 (2015).

[6] M. T. Mitchison, M. P. Woods, J. Prior, and M. Huber, New J. Phys. **17**, 115013 (2015).

[7] R. Uzdin, A. Levy, and R. Kosloff, Phys. Rev. X **5**, 031044 (2015).

[8] L. A. Correa, J. P. Palao, D. Alonso, and G. Adesso, Sci. Rep. **4**, 3949 (2014).

[9] D. Gelbwaser-Klimovsky, W. Niedenzu, P. Brumer, and G. Kurizki, Sci. Rep. **5**, 14413 (2015).

[10] R. Dillenschneider and E. Lutz, Europhys. Lett. **88**, 50003 (2009).

[11] T. Zhang, W.-T. Liu, P.-X. Chen, and C.-Z. Li, Phys. Rev. A **75**, 062102 (2007).

[12] F. Altintas, A. Ü. C. Hardal, and Ö. E. Müstecaplıoğlu, Phys. Rev. A **91**, 023816 (2015).

[13] A. Hewgill, A. Ferraro, and G. De Chiara, Phys. Rev. A **98**, 042102 (2018).

[14] J. B. Brask and N. Brunner, Phys. Rev. E **92**, 062101 (2015).

[15] N. Brunner, M. Huber, N. Linden, S. Popescu, R. Silva, and P. Skrzypczyk, Phys. Rev. E **89**, 032115 (2014).

[16] J. J. Park, K.-H. Kim, T. Sagawa, and S. W. Kim, Phys. Rev. Lett. **111**, 230402 (2013).

[17] M. O. Scully, M. S. Zubairy, G. S. Agarwal, and H. Walther, Science **299**, 862 (2003).

[18] J. Roßnagel, O. Abah, F. Schmidt-Kaler, K. Singer, and E. Lutz, Phys. Rev. Lett. **112**, 030602 (2014).

[19] X. L. Huang, T. Wang, and X. X. Yi, Phys. Rev. E **86**, 051105 (2012).

[20] W. Niedenzu, V. Mukherjee, A. Ghosh, A. G. Kofman, and G. Kurizki, Nat. Commun. **9**, 165 (2018).

[21] R. J. de Assis, T. M. de Mendonça, C. J. Villas-Boas, A. M. de Souza, R. S. Sarthour, I. S. Oliveira, and N. G. de Almeida, Phys. Rev. Lett. **122**, 240602 (2019).

[22] C. Purkait and A. Biswas, Phys. Rev. E **107**, 054110 (2023).

[23] S. Chand, S. Dasgupta, and A. Biswas, Phys. Rev. E **103**, 032144 (2021).

[24] P. Abiuso and V. Giovannetti, Phys. Rev. A **99**, 052106 (2019).

[25] A. Das and V. Mukherjee, Phys. Rev. Res. **2**, 033083 (2020).

[26] S. Rahav, U. Harbola, and S. Mukamel, Phys. Rev. A **86**, 043843 (2012).

[27] K. E. Dorfman, D. Xu, and J. Cao, Phys. Rev. E **97**, 042120 (2018).

[28] S. Çakmak, F. Altintas, A. Gençten, and Ö. E. Müstecaplıoğlu, Eur. Phys. J. D **71**, 75 (2017).

[29] D. Türkpençe and F. Altintas, Quant. Info. Proc. **18**, 255 (2019).

[30] B. Çakmak and Ö. E. Müstecaplıoğlu, Phys. Rev. E **99**, 032108 (2019).

[31] F. Plastina, A. Alecce, T. J. G. Apollaro, G. Falcone, G. Francica, F. Galve, N. Lo Gullo, and R. Zambrini, Phys. Rev. Lett. **113**, 260601 (2014).

[32] Y. Rezek, Entropy **12**, 1885 (2010).

[33] D. Loss and D. P. DiVincenzo, Phys. Rev. A **57**, 120 (1998).

[34] F. Meier, J. Levy, and D. Loss, Phys. Rev. Lett. **90**, 047901 (2003).

[35] G. Thomas and R. S. Johal, Phys. Rev. E **83**, 031135 (2011).

[36] S. Çakmak, F. Altintas, and Ö. E Müstecaplıoğlu, Eur. Phys. J. Plus **131**, 1 (2016).

[37] F. Altintas and Ö. E. Müstecaplıoğlu, Phys. Rev. E **92**, 022142 (2015).

[38] S. Çakmak, D. Türkpençe, and F. Altintas, Eur. Phys. J. Plus **132**, 554 (2017).

[39] X. Huang, Y. Liu, Z. Wang, and X. Niu, Eur. Phys. J. Plus **129**, 4 (2014).

[40] E. A. Ivanchenko, Phys. Rev. E **92**, 032124 (2015).

[41] A. Das and S. Ghosh, Entropy **21**, 1131 (2019).

[42] S. Chand and A. Biswas, Phys. Rev. E **95**, 032111 (2017).

[43] C. Purkait and A. Biswas, Phys. Lett. A **442**, 128180 (2022).

[44] A. C. Duriez, D. Martínez-Tibaduiza, and A. Z. Khoury, Phys. Rev. A **106**, 062212 (2022).

[45] A. Dodonov, D. Valente, and T. Werlang, J. Phys. A: Math. Theor. **51**, 365302 (2018).

[46] F. Altintas, A. U. C. Hardal, and O. E. Müstecaplıoğlu, Phys. Rev. E **90**, 032102 (2014).

[47] I. M. Georgescu, S. Ashhab, and F. Nori, Rev. Mod. Phys. **86**, 153 (2014).

[48] F. Kranzl, S. Birnkammer, M. K. Joshi, A. Bastianello, R. Blatt, M. Knap, and C. F. Roos, Phys. Rev. X **13**, 031017 (2023).

[49] D. Porras and J. I. Cirac, Phys. Rev. Lett. **92**, 207901 (2004).

[50] G. L. Kamta and A. F. Starace, Phys. Rev. Lett. **88**, 107901 (2002).

[51] G. Rigolin, Int. J. Quantum. Inform. **02**, 393 (2004).

[52] L. Zhou, H. S. Song, Y. Q. Guo, and C. Li, Phys. Rev. A **68**, 024301 (2003).

[53] Y. Guo-Hui, G. Wen-Bin, Z. Ling, and S. He-Shan, Commun. Theor. Phys. **48**, 453 (2007).

[54] Z. Hu, S. Youn, K. Kang, and C. Kim, J. Phys. A: Math. Gen. **39**, 10523 (2006).

[55] M. Rojas, S. de Souza, and O. Rojas, Ann. Phys. **377**, 506 (2017).

[56] Y. Yeo, T. Liu, Y.-E. Lu, and Q.-Z. Yang, J. Phys. A: Math. Gen. **38**, 3235 (2005).

[57] Y. Zhou and G.-F. Zhang, Eur. Phys. J. D **47**, 227 (2008).

[58] S. Haddadi, M. R. Pourkarimi, Y. Khedif, and M. Daoud, Eur. Phys. J. Plus **137**, 66 (2022).

[59] S. Ghosh and A. Sen De, Phys. Rev. A **105**, 022628 (2022).

[60] S. Ghosh, T. Chanda, and A. Sen De, Phys. Rev. A **101**, 032115 (2020).

[61] T. K. Konar, L. G. C. Lakkaraju, and A. S. De, arXiv:2203.09497.

[62] M. Y. Abd-Rabbou, A. ur Rahman, M. A. Yurischev, and S. Haddadi, Phys. Rev. E **108**, 034106 (2023).

[63] X. L. Huang, L. C. Wang, and X. X. Yi, Phys. Rev. E **87**, 012144 (2013).

[64] C. Cherubim, F. Brito, and S. Deffner, Entropy **21**, 545 (2019).

[65] L.-M. Zhao and G.-F. Zhang, Quant. Info. Proc. **16**, 216 (2017).

[66] S. Sonkar and R. S. Johal, Phys. Rev. A **107**, 032220 (2023).

[67] A. El Makouri, A. Slaoui, and M. Daoud, J. Phys. B: At. Mol. Opt. Phys. **56**, 085501 (2023).

[68] S. Suzuki, J.-i. Inoue, and B. K. Chakrabarti, *Quantum Ising Phases and Transitions in Transverse Ising Models* (Springer, Berlin, Heidelberg, 2012), Vol. 862.

[69] L. Buffoni, A. Solfanelli, P. Verrucchi, A. Cuccoli, and M. Campisi, Phys. Rev. Lett. **122**, 070603 (2019).

[70] A. Solfanelli, M. Falsetti, and M. Campisi, Phys. Rev. B **101**, 054513 (2020).

[71] J. R. Johansson, P. D. Nation, and F. Nori, Comput. Phys. Commun. **183**, 1760 (2012).

[72] P. Salamon, K. H. Hoffmann, Y. Rezek, and R. Kosloff, Phys. Chem. Chem. Phys. **11**, 1027 (2009).

[73] M. V. Berry, J. Phys. A: Math. Theor. **42**, 365303 (2009).

[74] Y. Rezek, P. Salamon, K. H. Hoffmann, and R. Kosloff, Europhys. Lett. **85**, 30008 (2009).

[75] A. Insinga, B. Andresen, and P. Salamon, Phys. Rev. E **94**, 012119 (2016).

[76] P. A. Camati, J. F. G. Santos, and R. M. Serra, Phys. Rev. A **99**, 062103 (2019).

[77] H.-P. Breuer and F. Petruccione, *The Theory of Open Quantum Systems* (Oxford University Press on Demand, 2002).

[78] T. D. Kieu, Phys. Rev. Lett. **93**, 140403 (2004).

[79] F. Wu, J. He, Y. Ma, and J. Wang, Phys. Rev. E **90**, 062134 (2014).

[80] F. L. Curzon and B. Ahlborn, Am. J. Phys. **43**, 22 (1975).

[81] P. Hess, P. Becker, H. Kaplan, A. Kyprianidis, A. Lee, B. Neyenhuis, G. Pagano, P. Richerme, C. Senko, J. Smith *et al.*, Philos. Trans. R. Soc. A **375**, 20170107 (2017).

[82] T. Graß and M. Lewenstein, EPJ Quantum Technol. **1**, 8 (2014).

[83] C. Monroe, W. C. Campbell, L.-M. Duan, Z.-X. Gong, A. V. Gorshkov, P. W. Hess, R. Islam, K. Kim, N. M. Linke, G. Pagano, P. Richerme, C. Senko, and N. Y. Yao, Rev. Mod. Phys. **93**, 025001 (2021).

[84] C. Monroe, W. Campbell, E. Edwards, R. Islam, D. Kafri, S. Korenblit, A. Lee, P. Richerme, C. Senko, and J. Smith, in *Proceedings of the International School of Physics "Enrico Fermi," Course 189* (IOS Press, Amsterdam, 2015), pp. 169–187.

[85] C. Cherubim, T. R. de Oliveira, and D. Jonathan, Phys. Rev. E **105**, 044120 (2022).